Dynamic Crack Curving—A Photoelastic Evaluation

by M. Ramulu and A.S. Kobayashi

ABSTRACT—A dynamic-crack-curving criterion, which is valid under pure Mode I or combined Modes I and II loadings and which is based on either the maximum circumferential stress or minimum strain-energy-density factor at a reference distance of r_0 from the crack tip, is verified with dynamic-photoelastic experiments. Directional stability of a Mode I crack propagation is attained when $r_0 = \frac{1}{128\pi}\left(\frac{K_I}{\sigma_{ox}}\right)^2 V_0^2(c, c_1, c_2) > r_c$, where r_c = 1.3 mm for Homalite-100 used in the dynamic-photoelastic experiments.

Introduction

Crack extension and fracture criteria under combined tension and shear loading are based on either energy or maximum circumferential-stress criteria. The maximum circumferential-stress, $\sigma_{\theta\theta}$, criterion was first used by Erdogan and Sih,[1] for predicting the direction, θ_c, of an angled crack. Williams and Ewing[2] extended this theory by incorporating the second-order term of σ_{ox} in the Williams eigenfunction expansion. Finnie and Saith[3] corrected an oversight in the above angle crack analysis and obtained an improved agreement between predicted and experimental data. Streit and Finnie[4] further proposed a crack-stability model where directional stability of a Mode I crack propagation is maintained when a characteristic distance of r_0 from the crack tip satisfies $r_0 \geq r_c$, where r_c is a critical distance ahead of the crack tip. Cotterell and Rice[5] derived the necessary condition for a slightly curved, quasi-static, mixed-mode crack growth where stability of crack growth was also governed by σ_{ox}. Karihaloo *et al.*[6] recently showed that crack curving can occur without kinking under vanishing σ_{ox} and Mode II stress-intensity factor, but with nonvanishing derivative of K_{II} with respect to the crack length.

As for the energy approach, Hussain *et al.*,[7] Palaniswamy and Knauss,[8] Gupta,[9] Wu,[10] and Nemat-Nasser *et al.*,[11-12] among others, predicted the direction of a kinked crack based on a maximum strain-energy release-rate criterion. Sih,[13] on the other hand, proposed the S-theory where the direction of crack kinking coincides with the direction of the minimum strain-energy density. Theocaris and Andrianopoulos[14] recently modified the S-theory by designating its mean value, $\bar{S}$, the critical quantity for crack initiation, under mixed-mode crack-tip deformation.

M. Ramulu (SESA Member) is Research Assistant Professor and A.S. Kobayashi (SESA Fellow) is Professor, University of Washington FU-10. Department of Mechanical Engineering, Seattle, WA 98195.

Paper was presented at SESA Spring Meeting held on Oahu and Maui, HI on May 24-28, 1982.

Original manuscript submitted: November 11, 1981. Authors notified of acceptance: June 21, 1982. Final version received: April 19, 1982.

The above papers all relate to quasi-static crack extension. As for dynamic-crack-curving criterion, Yoffe[15] and Sih[16] used the maximum dynamic-circumferential-stress theory and minimum strain-energy-density theory, respectively, to explain crack-branching phenomena.

The objective of the present study is to derive a dynamic-crack-curving criterion applicable to both Mode I and combined Modes I and II crack-tip deformation. In particular, dynamic extensions of two modified static-crack-curving criteria, that is the maximum circumferential stress and the minimum strain-energy-density criteria at a critical distance r_c, were considered. The developed theoretical relations were evaluated numerically and the influence of σ_{ox} and crack velocity on crack-curving direction were deduced. Crack-curving angles predicted by the two dynamic-crack-curving criteria were then compared with experimental results, obtained from past dynamic-photoelastic investigation.

Dynamic Crack-curving Criteria

Elastodynamic-crack-tip Stress Field

The dynamic-crack-curving criteria are derived from the near-field, mixed-mode elastodynamic state of stress associated with a crack tip propagating at constant velocity. This dynamic state of stress is given by Freund[17,18] in terms of local rectangular and polar coordinates of (x, y) and (r, θ), respectively, with origin at the crack tip, and the Mode I and II dynamic-stress-intensity factors, K_I and K_{II}*, respectively. The authors[19] have added to Freund's near-field, dynamic state of stress the second-order term of σ_{ox} which is acting parallel to the direction of crack extension. This dynamic-singular-crack-tip stress field under mixed-mode loading for small θ values differs from the corresponding static stress field in that the largest principal singular tensile stress acts parallel to the x axis, a fact which not only contributes to crack curving but also to dynamic crack branching. Furthermore, this region ahead of the running crack where $|\sigma_{xx}| > \sigma_{yy}$ increases with increases in crack speed and σ_{ox} even under pure Mode II crack-tip deformation.[19] This inevitable involvement of σ_{ox} forms the basis of incorporating σ_{ox} in the dynamic-crack-curving criteria presented in this paper.

Maximum Circumferential-stress Theory

The angle, θ_c, at which circumferential stress, $\sigma_{\theta\theta}$, is maximum, can be obtained from the following

**The superscript 'dyn' to identify dynamic-stress-intensity factor will not be used in this paper, since all quantities refer to dynamic values.*

$$\frac{\partial \theta_{\theta\theta}}{\partial \theta} = 0 \qquad \sigma_{\theta\theta} > 0 \qquad (1)$$

where the added $\sigma_{\theta\theta} > 0$ is to assure fracture in tension under mixed-mode loading.* For a pure Mode I dynamic-crack-tip state of stress eq (1) will yield a transcendental relation between the critical values of θ and r.

$$r = \frac{1}{4\pi}\left[\left(\frac{K_I}{\sigma_{\delta x}}\right) V(\theta, c, c_1, c_2)\right]^2 \qquad (2a)$$

Furthermore, by setting $\theta = 0$ in eq (2a), we obtain

$$r_0 = \frac{1}{128\pi}\left[\left(\frac{K_I}{\sigma_{ox}}\right) V_0(c, c_1, c_2)\right]^2 \qquad (2b)$$

and

$$V_0(c, c_1, c_2) = [B_1(c)\{-(1 + S_2^2)(2 - 3S_1^2) - \frac{4S_1S_2}{1 + S_2^2}(14 + 3S_2^2) - 16S_1(S_1 - S_2) + 16(1 + S_1^2)\}] \qquad (2c)$$

where

$$B_1(c) = \frac{(1 + S_2^2)}{[4S_1S_2 - (1 + S_2^2)^2]} \qquad (2d)$$

$$S_1^2 = [1 - \frac{c^2}{c_1^2}], \quad S_2^2 = 1 - [\frac{c^2}{c_2^2}] \qquad (2e)$$

and c, c_1 and c_2 are the crack velocity, dilatational wave velocity, and distortional wave velocity, respectively. It can be easily shown that for zero crack velocity or $c = 0$, eq (2b) reduces to Streit and Finnie's solution[4] of $r_0 = \frac{9}{128\pi}\left(\frac{K_I}{\sigma_{ox}}\right)^2$.

The exact form of eq (1) is too lengthy to reproduce here but can be found in Ref. 20.

Directional 'instability' is assumed to occur when the running crack deviates from its straight path at $r_0 \leq r_c$. Furthermore, r_c is assumed to be a material constant which can be determined experimentally by using eq (2b).

Figure 1 shows the velocity effect on r_0 which is plotted in a nondimensional form of $[\sqrt{r_0}\,\frac{\sigma_{ox}}{K_I}]$ for Mode I crack extension. Note that the dynamic r_0 is always less than the corresponding static r_0 for crack velocity of $0 < c \leq 0.325$ and is independent of the sign of σ_{ox}. The terminal crack velocity of $c/c_1 \mp 0.325$, in Fig. 1 where $r_0 = 0$ coincides with the terminal crack velocity predicted by Yoffe.[15]

Minimum Strain-energy-density Theory

According to this theory, the crack will extend to the location of the minimum strain-energy-density factor, S_{min}, or

$$\frac{\partial S}{\partial \theta} = 0 \text{ at } \theta = \theta_c \qquad (3)$$

The intensity of the strain-energy density, S, for the state of plane strain can be written as

$$S = r_0\frac{(1+\nu)}{2E}[(1-\nu)(\sigma_{xx}^2 + \sigma_{yy}^2) - 2\nu(\sigma_{xx} \cdot \sigma_{yy}) + 2\sigma_{xy}^2] \qquad (4)$$

where E and ν are the modulus of elasticity and Poisson's ratio, respectively. Substituting the dynamic-mixed-mode crack-tip stresses into eq (4) another lengthy equation relating K_I. K_{II}, σ_{ox}, r and θ is obtained.[20] Solving for r results in a transcendental relation, between r and θ, which varies with crack velocity.

By setting the Poisson's ratio $\nu = 1/3$, and $\sigma_{ox} = 0$ as the crack velocity $c \rightarrow 0$ in eq (3), the static angular prediction of crack curving described in Ref. 13 is recovered. When a nonvanishing second-order term of σ_{ox} is considered, eq (3) yields four θ_c values, a pair for S_{max} and another pair of S_{min} for given values of c, K_{II}/K_I, r_0 and

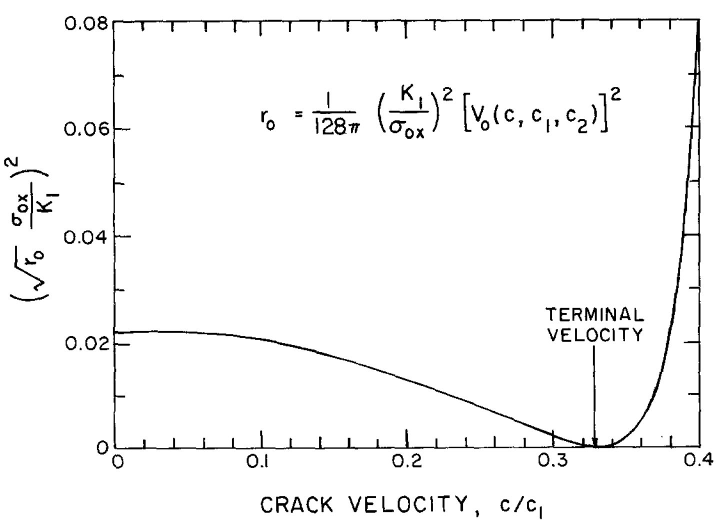

Fig. 1—Nondimensionalized remote stress vs. velocity for Mode I crack extension

σ_{ox}. Only the negative root of θ_c corresponding to positive K_{II}/K_I and the positive root of θ_c for negative K_{II}/K_I, under the tensile $\sigma_{\theta\theta}$ are of interest.[13]

Actual evaluation of eq (3) will show that curving of a straight crack propagating at the lower velocity can be considered only by incorporating the nonsingular term of σ_{ox} in the minimum strain-energy-density criteria. Such possibility of crack curving without K_{II} values and under the minimum strain-energy criterion has not been considered by others.

Comparison of Maximum $\sigma_{\theta\theta}$ and Minimum S Criterion

Figure 2 shows the predicted crack-curving angles for crack velocities, $0 \leq c/c_1 \leq 0.25$ by the maximum circumferential stress and the minimum strain-energy-density criteria with $\sigma_{ox} = 0$. Without the second-order term, both criteria predicted the same crack-curving angles for much of the crack-velocity range. Figure 2 also shows that for lower crack velocities of $c/c_1 \leq 0.15$, the predicted crack-curving angle, which is referred to as fracture angle from hereon, is almost equal to corresponding static fracture angles.

The effects of the nonsingular term of σ_{ox} and reference distance r_0, on the fracture angle predicted by both maximum $\sigma_{\theta\theta}$ and minimum S criteria at various crack velocities are shown in Fig. 3 for $\nu = 1/3$, and $K_{II}/K_I = -0.1$ and $\sigma_{ox}/K_I = -1.0$ and 1.0. Note that fracture angle for negative σ_{ox} is much smaller than those with positive σ_{ox}. Also, for a given tensile or compressive σ_{ox} larger r_0 results in larger fracture angle. Differences in fracture angles predicted by maximum circumferential-stress theory and minimum strain-energy-density theory increase with increased r_0 and crack velocity. Reference 14 discusses the influence of r_0 on the fracture angles.

Experimental Verification

Dynamic Isochromatics

For a single, pure Mode I or combined Modes I and II crack propagating at a constant velocity, the dynamic-crack-tip isochromatic patterns together with the predicted path are shown in Fig. 4. Changes in the remote stress, σ_{ox}, result in backward or forward tilting of the dynamic isochromatics. For a given σ_{ox}, the change in the sign of K_{II} results in a mirror image change in isochromatics. Detailed discussion of the changes in dyanmic isochromatics with variations in K_{II}/K_I and σ_{ox}/K_I can be found in Ref. 19.

Data-reduction Procedure

Dynamic isochromatics surrounding a running crack often exhibit moderate unsymmetry. Such photoelastic patterns were heretofore considered experimental abnormalities and were ignored by averaging the unsymmetric patterns during the data-reduction process. Careful postmortem inspection of the fracture specimens, however, show that higher σ_{ox} and slightly unsymmetric isochromatics are often associated with slightly curved crack patterns. With the development of a data-reduction procedure[19,21] for evaluating dynamic K_{II} together with K_I and σ_{ox}, it became possible to investigate the above criteria by extracting K_I, K_{II} and σ_{ox} from the previously recorded dynamic isochromatics surrounding running crack tips of curved cracks.

The dynamic-crack-curving criteria developed for pure Mode I loading conditions require accurate determination of K_I and σ_{ox}. Accuracy of the data-reduction procedure

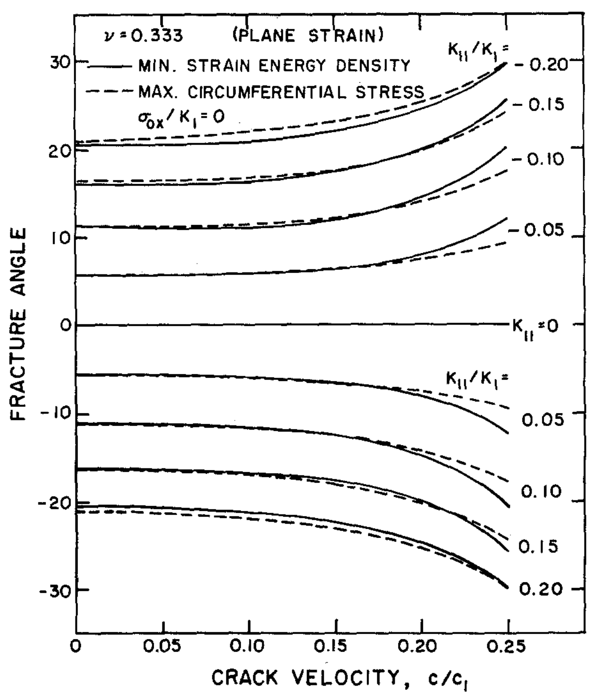

Fig. 2—Fracture angle predicted by maximum circumferential-stress criterion and minimum strain-energy-density criterion, $\sigma_{ox} = 0$

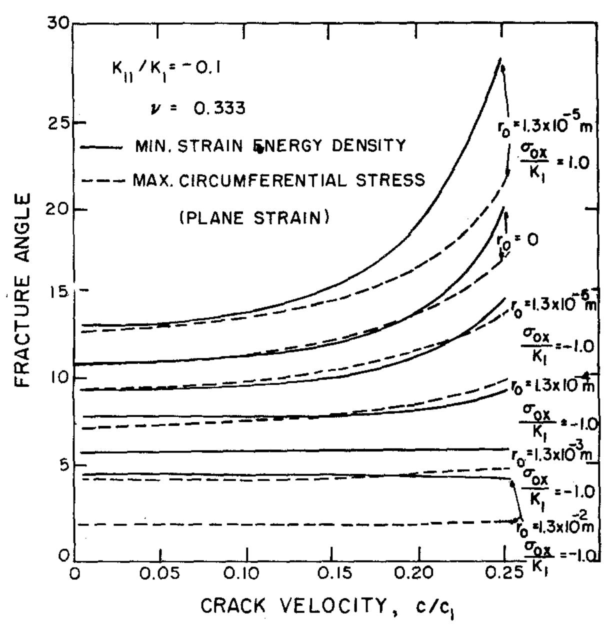

Fig. 3—Effects of r_o and σ_{ox} on fracture angle $K_{II}/K_I = -0.1$

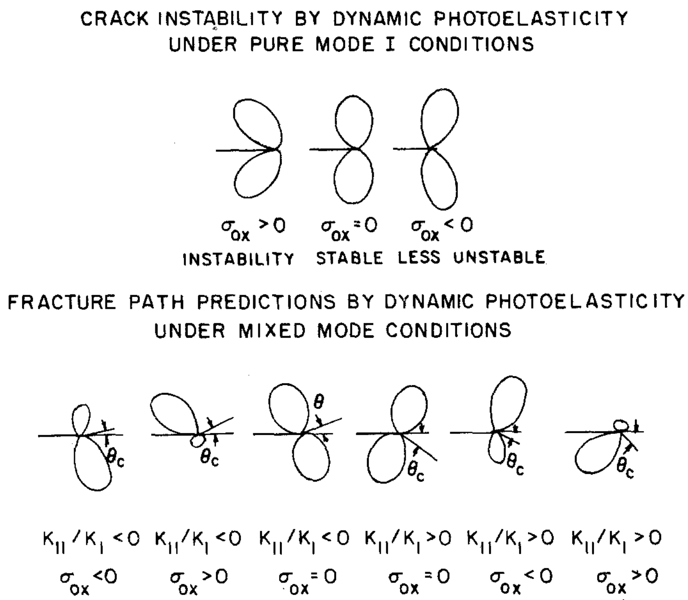

Fig. 4—Expected fracture paths by dynamic photoelasticity

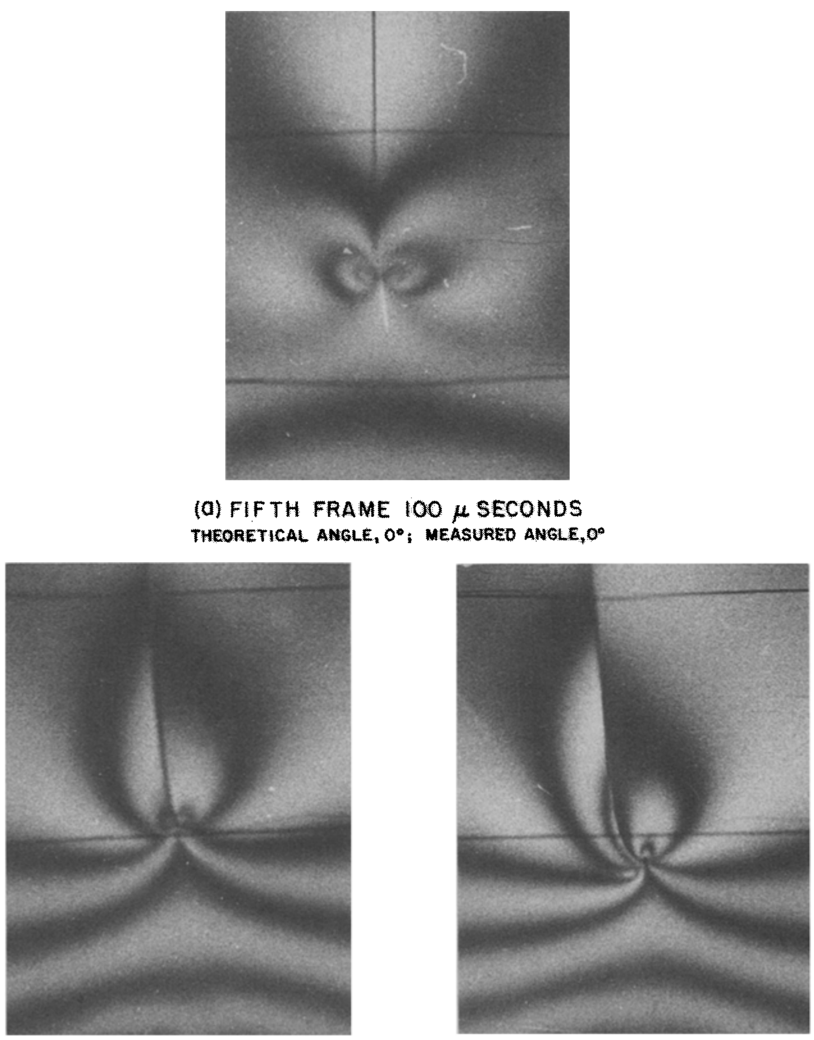

(a) FIFTH FRAME 100 μ SECONDS
THEORETICAL ANGLE, 0°; MEASURED ANGLE, 0°

(b) EIGTH FRAME 130 μ SECONDS
THEORETICAL ANGLE, 11°; MEASURED ANGLE, 11°

(c) TENTH FRAME 160 μ SECONDS
THEORETICAL ANGLE, 23°; MEASURED ANGLE 26°

Fig. 5—Typical dynamic isochromatics of a curved-crack Homalite-100 dynamic-tear-test (DTT) Specimen No. 6-C051074

used in this investigation was verified by using the above data-reduction procedure to calculate K_I and σ_{ox} from numerically generated isochromatics using the three parameters of K_I, σ_{ox}, and A_3 with $K_{II} = 0$.[22] The recovered two dynamic parameters K_I and σ_{ox} agreed within ±0.5 percent and ±5 percent, respectively, with the generated results. This series of numerical experiments showed that the two-parameter characterization procedure involving K_I and σ_{ox} describe reasonably well the stress field in the vicinity of a running crack tip.

The crack-curving angle was measured along the crack path by averaging the measured crack-curving angle at the front and back surfaces of the fractured specimen since the crack surfaces of some of the curved cracks were not perpendicular to the specimen surfaces. The maximum variation between the front and back crack-curving angles was about three degrees for severely curved cracks. Similar differences in out-of-phase crack curving were also observed by Williams *et al.* in their PMMA specimens.[2]

Results

Figure 5 shows three frames out of a 16-frame dynamic-photoelastic record of a curving crack in a Homalite-100 dynamic-tear-test (DTT) specimen of 9.5-mm (3/8-in.) thick, 88.9 × 400 mm (3½ × 15 in.). This beam with a blunt initial crack of 6.4-mm (7/32-in.) length was impact loaded by a drop weight of 1.48 kg (3.25 lb).[23] The crack emanated from the blunt saw-cut crack and propagated through much of the height of the beam prior to curving near the region of impact loading. Further details of the experimental setup, crack-velocity measurements and dynamic calibration of the Homalite-100 material used are found in Ref. 23. Figure 6 shows K_I, K_{II}, σ_{ox} and r_0, which is computed by eq (2), obtained from the dynamic-photoelastic pattern preceding and immediately after crack curving in Fig. 5. K_{II} is negligible at the point of instability and pronounced fluctuation in σ_{ox} is noted. After crack curving, K_{II} and σ_{ox} increased while K_I and the crack velocity dropped rapidly. r_0 was close to 1.5 mm in the continuously curving crack and reached a minimum value of $r_c \mp 1$ mm during the critical stage of crack curving.

Figure 7 shows a slightly curved crack and the associated K_I, K_{II}, σ_{ox} and r_0 in a fracturing 9.5-mm (3/8-in.) thick, 254 × 254 mm (10 × 10 in.) single-edged-notch (SEN) Homalite-100 specimen.[24] Gradual increase and decrease of K_I, a small K_{II} and rapid fluctuations in σ_{ox} and r_0 are noted. In the three SEN test results evaluated, K_I consistently reached a maximum value prior to crack curving, K_{II} was negligible and σ_{ox} always increased. At the onset of instability, K_I suddenly dropped, $K_{II} = 0$ and σ_{ox} increased. r_0 dropped sharply to an average value of 1.5 mm in all the three SEN-specimen data evaluated at the point of instability. This minimum r_0 value will be referred to r_c which will be found to be a material parameter associated with dynamic crack curving. A small K_{II} coexists immediately after crack instability, and changes the direction of crack propagation. A negative K_{II} immediately after instability resulted in a positive angle of crack curving. This result is not only in agreement with the analytically predicted angles in Fig. 3 but is also in agreement with similar observations in crack curving under stable-crack-growth conditions.[25] The rapid oscillations of r_0 in all the three SEN specimens appeared to be related to the rapid but opposing oscillations in σ_{ox}.

Figure 8 shows a curved crack and the associated K_I, K_{II}, σ_{ox} and r_0 in a Homalite-100, wedge-loaded, rectangular double-cantilever-beam (WL-RDCB) specimen of 9.5-mm (3/8-in.) thick and 76.2 × 152.4 mm (3 × 6 in.) with a blunt initial crack of length 2.4 mm (0.093 in.). Experimental details of this series of tests can be found in Ref. 26. Fluctuations in dynamic fracture parameters K_I, K_{II}, σ_{ox} and r_0 are noted all along the curved crack path. Immediately after the instability, a positive small K_{II}, associated with the large K_I resulted in a negative crack-curving angle. The crack curved continuously without any kinks and is characteristic of the fracture path in a DCB specimen.

Figure 9 shows five frames out of a 16-frame dynamic-photoelastic record of a curving crack in a 9.5-mm (3/8-in.) thick, 254 × 254 mm (10 × 10 in.) Homalite-100

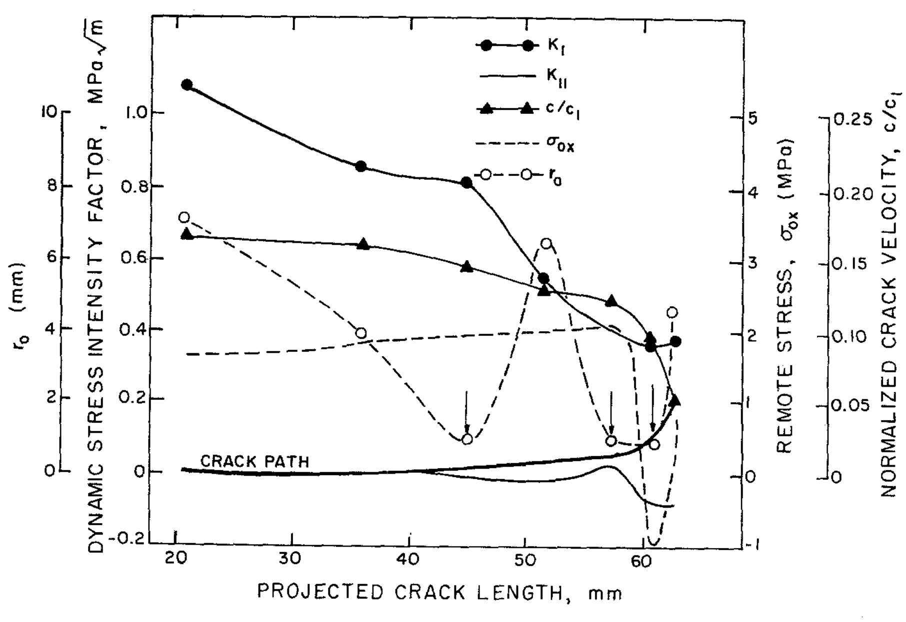

Fig. 6—Dynamic-fracture parameters associated with curved crack shown in Fig. 5

single-edge-notch (SEN) specimen loaded under fixed-gripped tension. The crack emanated from a small pre-crack 150 μs after impact by a flat-nosed projectile. The severe stress-wave reflections in this specimen caused the crack to curve continuously in a zig-zag manner. Details of this experiment can be found in Ref. 27. Figure 10 shows the corresponding K_I, K_{II}, σ_{ox} and r_0 variations associated with the unsymmetric dynamic isochromatics in this test. Severe stress-wave loading generated positive K_{II} and caused the crack to curve immediately after propagation. r_c is about 1.4 mm but σ_{ox} changed signs, resulting in a zig-zagged crack path.

Fracture angles of curved cracks measured in nine dynamic photoelasticity tests and the corresponding fracture angles computed by the maximum $\sigma_{\theta\theta}$ and minimum S theories are summarized in Table 1. Also, theoretically predicted and measured crack-curving angles are shown in Figs. 5 and 9, respectively. The remarkable agreements in experimentally measured and numerically computed results by both theories, using the experimentally determined $r_c \mp 1.3$ mm for Homalite-100, are noted. Crack-curving angles in our Mode I loading-condition experiments ranged between ±25 deg to a minimum of 2 deg for severe to moderate curving.

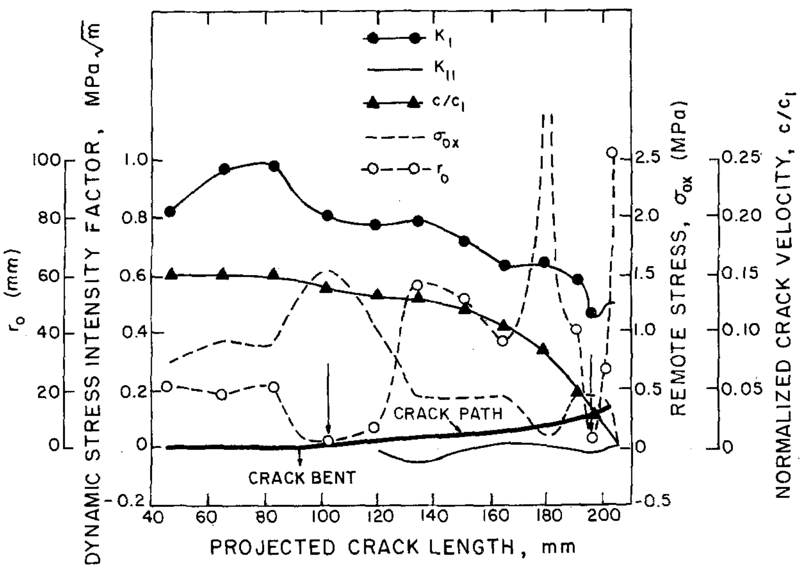

Fig. 7—Dynamic-fracture parameters associated with a slightly curved crack in a single-edge-notch (SEN) tension plate, Homalite-100, Specimen No. B12

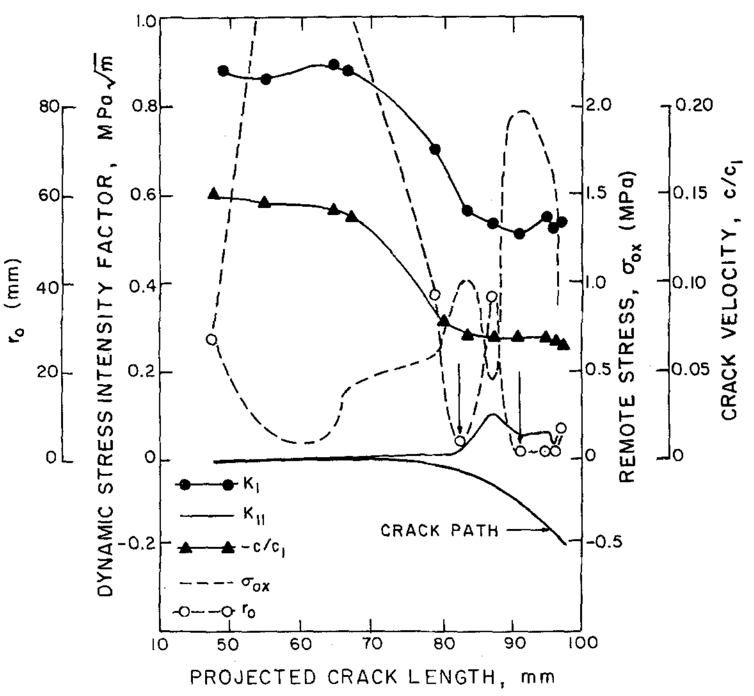

Fig. 8—Dynamic-fracture parameters associated with a curved crack in a wedge-loaded rectangular-double-cantilever (WL-RDCB) specimen, Homalite-100, Specimen No. L7B-051573

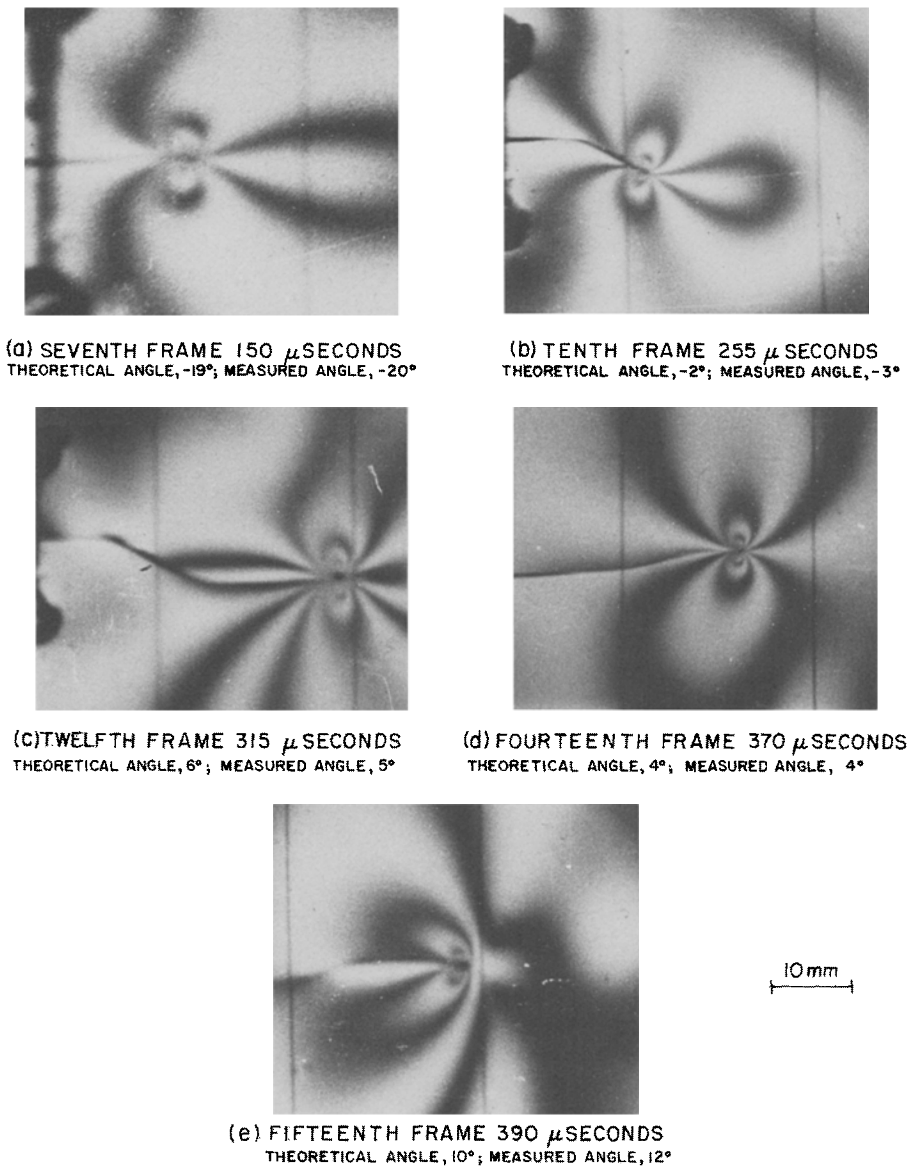

Fig. 9—Typical dynamic isochromatics of a curved crack. Homalite-100 single-edge-notch (SEN) specimen impacted by a flat-nose projectile, Specimen No. 21-W090771

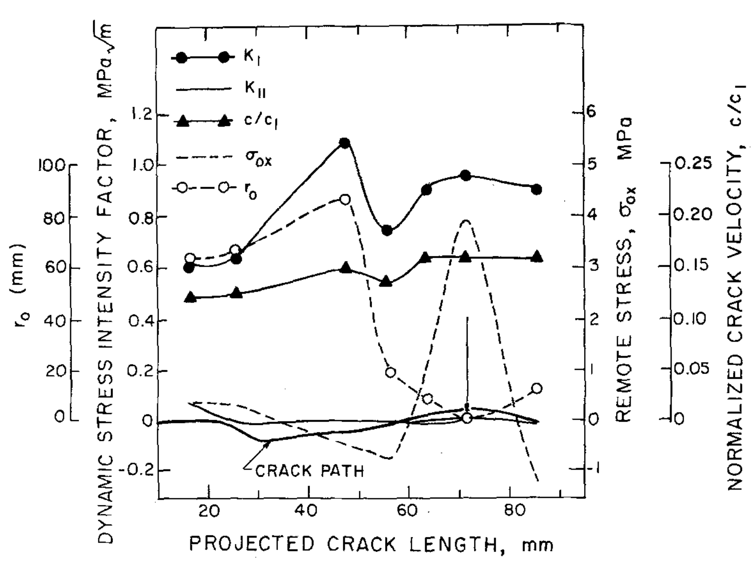

Fig. 10—Dynamic-fracture parameters associated with a curved crack shown in Fig. 9

Discussion

The closed-form elasticity solution for a circular-arc crack under uniform stress field provides a simple check on the accuracy of using the near-field solution of a straight crack in the results cited above. The static solution given by Panasyuk and Brezhnitskiy[28] in the vicinity of a circular-arc crack with an included angle 2α differ with straight-crack solution only by a multiplication factor of

$$K_I^{curved} = K_I^{straight} \cos \alpha/2/(1 + \sin^2 \alpha/2) \quad (6a)$$

$$K_{II}^{curved} = K_{II}^{straight} \sin \alpha/2/(1 + \sin^2 \alpha/2) \quad (6b)$$

$$\sigma_{ox}^{curved} = \sigma_{ox}^{straight} \sin^2 \alpha/2/(1 + \sin^2 \alpha/2) \quad (6c)$$

where the superscripts 'straight' and 'curved' refer to crack-tip parameters associated with a straight and curved crack, respectively. Possible errors, which were generated by fitting a straight-crack solution to a curved crack, were estimated. The procedure consisted of least-square fitting the exact solution of a curved crack and the corresponding solution for a straight crack to the two extreme curved cracks associated with the latest data points in Figs. 6 and 8. The resultant K_I, K_{II} and σ_{ox} of the straight-crack solutions are within 10 percent, 28 percent and 6 percent, respectively, of the corresponding solutions for circular-arc cracks of $\alpha \mp 25$ and 28 deg. Thus, possible error introduced by using a second-order dynamic-crack-tip state of stress of a straight crack in place of a curved crack should be negligible for most of the curved-crack problems of $\alpha \mp 5$ and 10 deg in this investigation.

Figure 11 illustrates the influence of σ_{ox} on the shape and tilting of the isochromatics. For a given $K_{II}/K_I = 0.1$ and crack velocity of $c/c_1 = 0.16$, a -0.1 to 0.1 variation in σ_{ox}/K_I will result in a six-percent variation in the maximum radial distance, r_{max}, and a ± 12-percent variation in the angle of tilt, θ_m, of the isochromatics. Conversely, should r_{max} and θ_m be measured within ± 6 percent and ± 12 percent, a range of $-0.1 < \sigma_{ox}/K_I < 0.1$ is to be expected.

Figure 12 shows an enlarged figure of the fifteenth frame of the recorded isochromatic patterns associated with the curved crack of Fig. 9. K_I, K_{II} and σ_{ox} were determined from isochromatic-fringe order of 3.5 for the curved crack. The accuracy in σ_{ox} determination can be estimated by comparing the calculated and recorded fringes of order 2.5. The coincidence is reasonable for a radial distance of about 5 mm (0.2 in.) and thus the error involved in σ_{ox} estimation is negligible.

The developed dynamic-crack-curving criterion shows that the large σ_{ox} contributes to crack instability and is in agreement with Benbow and Roesler's conclusion involving static experiments.[29] Cotterell[30–32] referring to Williams's

TABLE 1—SUMMARY OF EXPERIMENTAL AND THEORETICAL RESULTS

Total number of experiments:	9
Type of fracture specimen:	DTT, SEN, WL-RDCB
Number of data points:	81
Crack velocity, c/c_1:	0.03 to 0.21
K_I (MPa$\sqrt{m}$)	0.50 to 1.59
K_{II}/K_I	−0.22 to 0.18
σ_{ox}/K_I	−2.89 to 4.04
Experimental fracture angle associated with crack curving:	−20 deg to 26 deg
Theoretical prediction of fracture angle:	−20 deg to 25 deg
r_c (mm)	1.0 to 1.5

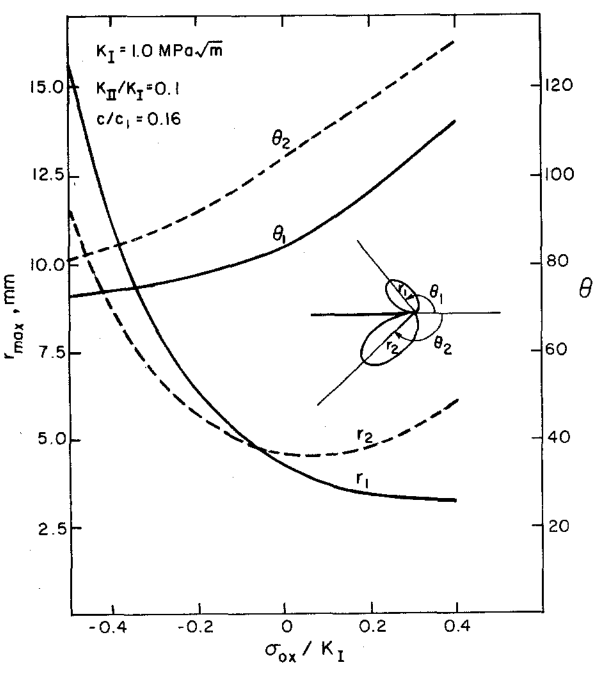

Fig. 11—Effect of σ_{ox} on the isochromatic fringe

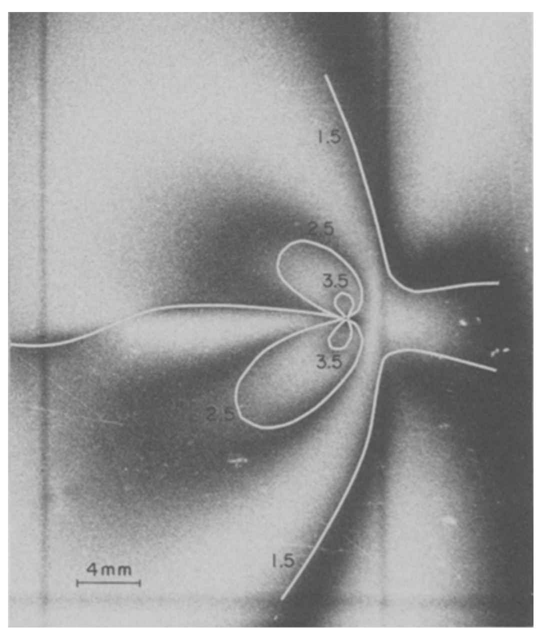

Fig. 12—Calculated and recorded isochromatics, 15th frame, 390 μs of Fig. 9

analysis,[33] showed that the crack path will be unstable when σ_{ox} is positive. The above static-crack-stability criterion[29-32] correlates well with the experimental results of DCB and CT specimens but cannot explain dynamic crack curvings in fracture specimens of SEN, and DTT where σ_{ox} is negative. The proposed criterion for the directional stability of a propagating crack is independent of the sign of the σ_{ox}, and is thus applicable to all crack-curving data considered in this paper.

As shown in Fig. 3 the influence of nonsingular stress is more pronounced for moderate values of r_0 irrespective of the sign of K_{II}/K_I. This result re-emphasizes the importance of the nonsingular stress term σ_{ox}, which, when neglected, can lead to inaccurate results as observed by Tirosh.[34]

Considering the fact that dynamic photoelasticity experiments cited in this paper were conducted by four different investigators over a period of ten years with different shipments of Homalite-100, the consistent results of $r_c \mp 1.3$ mm is noticeable. This magnitude of r_c at the onset of stability is larger than those reported in Refs. 2 and 11, which is due partly to the different material under consideration but mainly due to the ad hoc procedure in which r_c values were determined by others. In a critical review of r_c associated with the minimum S criterion of crack curving, Theocaris and Andrianopoulos[14] also determined experimentally $r_c = 1.3$ mm (0.05 in.) for polymethylmethacrylate.

Finally, the crack-curving criterion by Karihaloo *et al.*[12] requires that K_{II} be known immediately before and after crack curving. The lack of sensitivity in this analysis precluded precise variations of the very small K_{II} before or after crack curving and thus this crack curving could not be checked.

Conclusions

(1) A dynamic-crack-curving criterion based on the directional stability of a running crack at a critical distance

$$r_0 = 1/128\pi[(K_I/\sigma_{ox})V_o(c,c_1,c_2)]^2$$

under pure Mode I loading is developed. Directional stability is ensured when $r_0 > r_c$, where r_c is a critical material constant.

(2) Dynamic fracture angle under pure Mode I and mixed Mode I and II conditions can be predicted by using either the maximum circumferential-stress or the minimum strain-energy-density theories with the nonsingular stress term σ_{ox}. The difference in dynamic-crack-curving angles predicted by either theories nearly is equal for $\nu = 0.33$ to those of static analyses when $c/c_1 \leq 0.15$.

(3) Positive σ_{ox} always enhances the crack curving and negative σ_{ox} reduces the fracture angle irrespective of the sign of K_{II}/K_I.

(4) Experimental results with and without K_{II} proved that r_c is a material constant. The critical value of Homalite-100 is $r_c = 1.3$ mm (0.05 in.).

Acknowledgment

The results reported in this paper were obtained through ONR Contract No. 00014-76-C-0600 NR 64-478. The authors wish to thank N. Perrone and Yapa Rajapakse, ONR, for their support durmg the course of this investigation.

References

1. Erdogan, F. and Sih, G.C., "On the Crack Extension in Plates Under Plane Loading and Transverse Shear," Trans. ASME J. Basic Engrg. **85** (D), 519-527 (1963).
2. Williams, J.G. and Ewing, P.D., "Fracture Under Complex Stress - The Angled Crack Problem," Int. J. Fract. Mech., **8**, 441-446 (1972).
3. Finnie, I. and Saith, A., "A Note on the Angled Crack Problem and the Directional Stability of Crack," Int. F. Fract., **9**, 484-486 (1973).
4. Streit, R. and Finnie, I., "An Experimental Investigation of Crack-path Directional Stability," EXPERIMENTAL MECHANICS, **20** (1), 17-23 (Jan. 1980).
5. Cotterell, B. and Rice, J.R., "Slightly Curved or Kinked Cracks," Int. J. Frac., **11** (2), 155-164 (1981).
6. Karihaloo, B.L., Keer, L.M., Nemat-Nasser, S. and Oranatnachai, A., "Approximate Description of Crack Kinking and Curving," ASME Paper No. 81-APM-22.
7. Hussain, M.A., Pu, S.L. and Underwood, J., "Strain-Energy-Release Rate for a Crack Under Combined Mode I and Mode II," ASTM-STP-560, 2-28 (1974).
8. Palaniswamy, K. and Knauss, W.G., "On the Problem of Crack Extension in Brittle Solids Under General Loading," Mechanics Today, **4**, ed. S. Nemat-Nasser, Pergamon Press, 87-148 (1978).
9. Gupta, G.D., "Strain Energy Release Rate for Mixed Mode Crack Problem," ASME Paper No. 76-WA/PVP-7.
10. Wu, C.H., "Elasticity Problems of Slender Z-Crack," J. Elasticity, **8**, 183-205 (1978).
11. Hayashi, K. and Nemat-Nasser, S., "Energy Release Rate and Crack Kinking," Int. J. of Solids and Structures, **17**, 107-114 (1981).
12. Karihaloo, B.L., Keer, L.M. and Nemat-Nasser, S., "Crack Kinking Under Non-Symmetric Loading," Engrg. Fract. Mech., **13**, 879-888 (1980).
13. Sih, G.C., "A Special Theory of Crack Propagation," Methods of Analysis and Solutions of Crack Problems, **1**, ed. G.C. Sih, Noordhoff Inter. Publishing, Leyden, 21-45 (1973).
14. Theocaris, P.S. and Andrianopoulos, N.P., "A Modified Strain Energy Density Criterion Applied to Crack Propagation," J. Appl. Mech., **49** (1), 81-86 (1982).
15. Yoffe, E.H., "The Moving Griffith Crack," Phil. Mag., **42**, 739-750 (1951).
16. Sih, G.C., "Dynamic Crack Problems: Strain Energy Density Fracture Theory," Elastodynamic Crack Problems, **4**, ed. G.C. Sih, Noordhoff Inter. Publishing, Leyden, 17-37 (1977).
17. Freund, L.B., "Dynamic Crack Propagation," The Mechanics of Fracture, **19**, ed. by F. Erdogan, ASME, 105-134 (1976).
18. Freund, L.B., "The Mechanics of Dynamic Shear Crack Propagation," J. Geophysical Res., **84** (35), 2199-2209 (1978).
19. Kobayashi, A.S. and Ramulu, M., "Dynamic Stress-intensity Factors for Unsymmetric Dynamic Isochromatics," EXPERIMENTAL MECHANICS, **21** (1), 41-48 (Jan. 1981).
20. Ramulu, M., "Dynamic Crack Curving and Branching," doctoral thesis submitted to the Univ. of Washington (March 1982).
21. Kobayashi, A.S. and Ramulu, M., "Dynamic Mixed Mode Fracture," Proc. U.S.-Greece Symp. on Mixed Mode Fracture, ed. G. Sih and P.S. Theocaris, Noordhoff, Holland (1981).
22. Kobayashi, A.S. and Mall, S., "Dynamic Fracture Toughness of Homalite-100," EXPERIMENTAL MECHANICS, **18** (1), 11-18 (Jan. 1978).
23. Kobayashi, A.S. and Chan, C.F., "A Dynamic Photoelastic Analysis of Dynamic-tear-test Specimen," EXPERIMENTAL MECHANICS, **16** (5), 176-181 (May 1976).
24. Bradley, W.B. and Kobayashi, A.S., "Fracture Mechanics - A Photoelastic Investigation," Engrg. Frac. Mech., **3**, 317-332 (1971).
25. Iida, S. and Kobayashi, A.S., "Crack Propagation Rate in 7075-T6 Plates Under Cyclic Tensile and Transverse Shear Loading," J. Basic Engrg., Trans. of ASME, **91**, Series D (4), 764-769 (Dec. 1964).
26. Kobayashi, A.S., Mall, S. and Lee, M.H., "Fracture Dynamics of Wedge-Loaded Double Cantilever Beam Specimen," Cracks and Fracture, ASTM STP, 601, 274-290 (June 1976).
27. Wade, B.G. and Kobayashi, A.S., "Photoelastic Investigation on the Crack Arrest Capability of Pretensioned Stiffened Panels," EXPERIMENTAL MECHANICS, **15** (1), 1-9 (1975).
28. Panasyuk, V.V. and Brezhnitskiy, L.T., Voprosy Mechaniki, Real nogo Tverdogo Tela No. 3, Naukova Dumka Press, Kiev (1965).
29. Benbow, J.J. and Roesler, F.C., "Experiments on Controlled Fractures," Proc. Phys. Soc., **70**, Ser. B, 201-211 (1957).
30. Cotterell, B., "Notes on the Paths and Stability of Cracks," Int. J. Frac. Mech., **2**, 526-533 (1966).
31. Cotterell, B., "On Fracture Path Stability in the Compact Tension Test," Int. J. Frac. Mech., **6**, 189-192 (1970).
32. Cotterell, B., "On Brittle Fracture Paths," Int. J. Frac. Mech., **1**, 96-103 (1965).
33. Williams, M.L., "On the Stress Distribution at the Base of a Stationary Crack," J. Appl. Mech., **24**, 109-116 (1957).
34. Tirosh, J., "Incipient Fracture Angle, Fracture Loci and Critical Stress for Mixed Mode Loading," Eng. Frac. Mech., **9**, 607-616 (1977).